LBM simulation of free convection in a nanofluid filled incinerator containing a hot block

Mohamed Ammar Abbassi, Mohammad Reza Safaei, Ridha Djebali, Kamel Guedri, Belkacem Zeghmati, Abdullah A.A.A. Alrashed

LBM simulation of free convection in a nanofluid filled incinerator containing a hot block

Mohamed Ammar Abbassi [a], Mohammad Reza Safaei [bc,*], Ridha Djebali [ad], Kamel Guedri [e], Belkacem Zeghmati [f], Abdullah A.A.A. Alrashed [g]

[a] UR: Unité de Recherche Matériaux, Energie et Energies Renouvelables (MEER), Faculté des Sciences de Gafsa, B.P.19, Zarroug, Gafsa 2112, Tunisia
[b] Division of Computational Physics, Institute for Computational Science, Ton Duc Thang University, Ho Chi Minh City, Vietnam
[c] Faculty of Electrical and Electronics Engineering, Ton Duc Thang University, Ho Chi Minh City, Vietnam
[d] Renewable Energies for Agriculture and Agro-Industry (ERAAI), ESIM, University of Jendouba, Tunisia
[e] Mechanical Engineering Department, College of Engineering and Islamic Architecture, Umm Al-Qura University, KSA
[f] LAMPS: Université de Perpignan Via Domitia, 52 avenue Paul Alduy, 66860 Perpignan Cedex, France
[g] Department of Automotive and Marine Engineering Technology, College of Technological Studies, The Public Authority for Applied Education and Training, Kuwait

The present study explores nanofluid magnetohydrodynamics (MHD) natural convection in an incinerator shaped enclosure including a rectangular hot block situated on the bottom wall. A parametric investigation is conducted to explore the effect of different parameters such as nanoparticles volume fraction ($\phi = 0$–4%), Rayleigh number ($Ra = 10^3$–10^5), external magnetic field intensity ($Ha = 0$–100), incinerator tilting angle ($\gamma = 0$–360°) and hot block's height (0.1–0.5), width (0.1–0.8) and position on heat transfer, nanofluid flow, and entropy generation inside the incinerator. The top and bottom horizontal walls of enclosure are adiabatic; the right, left vertical and inclined walls are supposed to have cold temperature whereas the hot block is maintained at a hot temperature. The Brownian motion was also considered in calculating the effective nanofluid thermal conductivity and viscosity using Koo–Kleinstreuer–Li (KKL) correlation. The lattice-Boltzmann method is used with a D2Q9-D2Q9 double population's model as utilized CFD approach. The mesh independency study and the validation of proposed model are accomplished in several cases and very good agreement is found between present results and former experimental and numerical findings. The results showed that entropy generation is augmented by increasing height and width of heater, nanoparticles volume fraction and Rayleigh number but it is reduced by enhacing Hartmann number. However, increasing the magnetic field does not have notable influence on heat transfer, compared to other parameters. The optimum incinerator inclination angles to maximize heat transfer and minimize entropy generation are 90° and 270°.

1. Introduction

Control of heat transfer is crucial in energy generating systems. Various techniques of heat transfer augmentation have been proposed in the literature focusing on optimizing the geometry, swirl flow devices, use of porous media, partitioned cavities and etc., which are well documented [1]. Bergles [2] classified the techniques of heat transfer enhancement as active or passive. Active methods need external power to preserve the improvement mechanism, yet passive improvement techniques do not require external power. An advanced way of heat transfer improvement consists of using a base fluid with nanoparticles of superior thermal conductivities suspended inside. The procured solution is named nanofluid which is presented first time by Choi and Eastman [3] is classified among the passive improvement techniques. According to Safaei et al. [4], nanofluids are mixtures formed by solid–liquid that consists of a base liquid and nanoparticles (particles with diameters less than 100 nm). Nanoparticles are fundamentally metal (Cu [5], Ag [6], Co [7], etc.), oxides (CuO [8], ZnO [9], Al_2O_3 [10], TiO_2 [11], Fe_2O_3 [12], SiO_2 [13], etc.) and some other compounds like graphene [14], single-walled [15], double-walled [16] or multi-walled [17] carbon nanotubes, diamond [18], etc. whereas base fluid frequently includes water [19], propylene glycol [20], ethylene glycol [21] and oil [22]. Nanofluids behave such normal, current working fluids-due to the small size of nanoparticles-compared to other techniques used for improving heat transfer in industrial applications. This technique can be used for the thermal machines which will be constructed in the future or even for the ones which are already functioning with little modifications [23].

* Corresponding author at: Faculty of Electrical and Electronics Engineering, Ton Duc Thang University, Ho Chi Minh City, Vietnam
E-mail address: cfd_safaei@tdt.edu.vn (M.R. Safaei).

Nomenclature

B_0	magnetic field, T
c	lattice velocity, m s^{-1}
c_s	speed of the sound, m s^{-1}
c_i	discrete particle speed, m s^{-1}
C_p	specific heat at constant pressure, J K^{-1} kg^{-1}
F_i	external forces, N
f	density distribution functions, kg m^{-3}
f^{eq}	equilibrium density distribution functions, kg m^{-3}
g^{eq}	internal energy distribution functions, K
H	incinerator height, m
Ha	hartmann number
g^{eq}	equilibrium internal energy distribution functions, K
g	gravity acceleration, m s^{-2}
k	thermal conductivity, W K^{-1} m^{-1}
Ma	Mach number
L	incinerator width, m
m	number of lattices in y direction
Nu	local Nusselt number
n	number of lattices in x direction
P	pressure, N m^{-2}
Pr	Prandtl number
Ra	Rayleigh number
S_{gen}	entropy generation, J K^{-1}
T	temperature, K
$\mathbf{u}(u, v)$	velocities, m s^{-1}
$\mathbf{x}(x, y)$	lattice coordinates, m

Greek symbols

α	thermal diffusivity, m^2 s^{-1}
β_T	thermal expansion coefficient, K^{-1}
γ	incinerator inclination angle
θ	non-dimensional temperature
μ	dynamic viscosity, kg m^{-1} s^{-1}
ν	kinematic viscosity, m^2 s^{-1}
ρ	density, kg m^{-3}
σ	electrical conductivity, S m^{-1}
ϕ	solid volume fraction
τ_α	relaxation time for flow, s
τ_ν	relaxation time for temperature, s
Δx	lattice spacing, m
Δt	time increment, s
ψ	non-dimensional stream function
ω_i	weighting factor for flow
ω_i'	weighting factor for temperature
Δ	difference

Subscript

f	fluid
nf	nanofluid
p	particle
h	hot
c	cold
static	static

A review of recent researches made with nanofluids can be found in Solangi et al. [24].

On the other hand, natural convection heat transfer due to a localized heat source in complex geometries is ubiquitous in the majority of industrial systems. It has been studied extensively because of its interest in many practical systems including cooling of electronic equipment [25], chimneys [26], heat exchangers [27], solar collectors [28], nuclear engineering [29], power plants [30], building engineering [31] and geophysical flows [32]. Sarris et al. [33] numerically investigated free convection in rectangular tanks heated locally from below, using a high Prandtl number fluid. Their results demonstrated that increasing the Rayleigh number develops a local temperature enhancement at the top of the heated strip without significant temperature increment in the cold tank sections. They also found that increasing the tank aspect ratio and the heated strip width enhances the fluid temperature and intensifies the fluid flow, which results in a more homogeneous glass melt and leads to a better quality of final product. Also, the heated strip position plays a vital role on the fluid flow, the temperature distribution and the thermal diffusion. Esfe et al. [34] numerically investigated the mixed convection heat transfer of water–alumina nanofluid in an inclined lid-driven square cavity with an interior hot obstacle. They concluded that the average Nusselt number augments by the Richardson number decrement for all studied nanoparticle concentration. Mliki et al. [35] studied the influence of nanoparticle Brownian motion on MHD free convection of CuO/H_2O nanofluid with uniform heat generation or absorption for a cavity with uniform or sinusoidally boundary conditions. They concluded that the Brownian motion is lessened at high Hartman or Rayleigh numbers. Also, they found the existing of a critical value for the nanoparticle volume fraction, when the Brownian motion is taken into consideration. Baïri et al. [36] made a review study on free convection in parallelogram-shaped cavities. They reviewed different shapes of cavities with considering various parameters such as cavity inclination, boundary conditions, thermal and radiative properties of the fluid and distributions of heat sources. In this regard, a critical study on various types of research methods such as experimental, numerical, analytical and inverse approaches has been carried out with a special focus on convective diode cavity. Saravanan and Sivaraj [37] numerically studied free convection in an air filled enclosure with a non-uniform heat flux which set up centrally on the bottom wall. Their results illustrated that the most influential parameters are the source length and Grashof number. Oztop et al. [38] reviewed free convection heat transfer and fluid flow in various enclosures by local heat sources. The main goal of their review paper was to survey the effect of the type and place of heat sources. They also studied the impacts of the various boundary conditions and configurations on the nanofluid flow and heat transfer of an enclosure, in their review paper. Natural convection heat transfer in enclosures with separate heat sources have been perused numerically as well as experimentally by studies in [39–42]. Paroncini and Corvaro [43] experimentally analyzed the convection heat transfer in an air filled square enclosure. Heat generation in the enclosure was performed by using a hot strip, located in the middle of enclosure, with three different heights. Their experiments showed that the natural convection heat transfer worsens with the source height increment. Mejri et al. [44] investigated laminar free convection and entropy generation of Al_2O_3/H_2O nanofluid in an enclosure, under a magnetic field. They used the Lattice Boltzmann Method (LBM) for the mathematical problem solving. They adjusted the controlling parameters in order to find conditions with maximum heat transfer and minimum entropy generation. Lately, a numerical investigation on free convection in a water filled inclined triangular cavity was made by Mejri et al. [45]. Their results showed that heat transfer rate augments with the increase of Rayleigh number. Minimum heat transfer is found for an inclination angle of 135° whereas for an inclination angle equal to zero, heat transfer is the highest. Mahmoudi et al. [46] studied free convection heat transfer and entropy generation in a cavity filled with Al_2O_3 nanoparticles, in presence of magnetic field. Their results revealed that for $Ra \leq 10^5$ and $Ha \leq 30$, heat generation/absorption coefficient has a great influence on transfer rate but it does not affect entropy generation for the studied values. Kefayati [47,48] studied the heat transfer and entropy generation of laminar free convection of non-Newtonian water/copper nanofluids in a square enclosure. He used the Finite Difference Lattice Boltzmann Method (FDLBM) as a numerical tool. The results of both studies showed that an augmentation of Rayleigh number or nanoparticles volume fraction increases heat transfer. Selimefendigil and Öztop [49] studied numerically MHD nanofluid free convection in an enclosure

with different shaped obstacles situated inside with uniform heat generation. They used the Galerkin weighted residual finite element method as a numerical tool. Their study demonstrated that the highest reduction of heat transfer is for the case of squared shaped obstacle, and the lowest is for the case of a circular obstacle.

In recent years, the Lattice Boltzmann Method (LBM) has introduced and utilized as a new, replete numerical technique, based on kinetic theory, for thermos-fluid phenomena modeling [50]. The benefits of LBM consist of simple computation procedures and ease in the implementation of boundary conditions [51]. It is worth noting LBM can be used easily for parallel computation, which is common in modeling of multiphase flow through complex geometries [52]. Besides, LBM modeling does not need any pressure-velocity coupling. In former techniques like FVM, this linkage is handled by an algorithm such as SIMPLER, SIMPLE, etc. which are CPU time consumers [53]. Another benefit is that it can simulate turbulent flows without using of any turbulence models [54]. More details on the LBM can be obtained in the reference books published on LBM [55,56].

The main objective of this research is to study the laminar natural convection heat transfer of nanofluid in incinerator shaped geometry. A heated block is located on the bottom wall of incinerator, whilst the top wall is assumed to be adiabatic and the vertical walls are presumed cold. The Lattice Boltzmann Method (LBM) is used to solve the governing equations. The grid sensitivity study and the validation of used model are made on simple cavity cases. The impacts of influential parameters (Rayleigh number, Hartman number, nanoparticle volume fraction, inclination angle, and hot source width, height and position) on flow, entropy generation, thermal fields and local as well as average Nusselt number are addressed. The result of present study would be useful for engineers and researchers who work on cooling of electronic devices like LED, VLSI circuits and MEMS [57].

2. Physical model and mathematical formulation

2.1. Governing equations

The studied physical domain is a two-dimensional incinerator shaped enclosure filled with aluminium oxide/water nanofluid as illustrated in Fig. 1. The hot block is situated at the bottom wall and maintained at high temperature. A uniform magnetic field ($\vec{B}_0 = B_0\vec{i}$) is applied as depicted in Fig. 1. The flow is considered to be incompressible, laminar, Newtonian and two-dimensional. Thermophysical properties are supposed to be constant, except density which is modeled through Boussinesq approximation. Further, the mixture of base fluid and spherical suspended nanoparticles are assumed as a single phase fluid with homogeneous effective properties. The magnetic force due to the weak magnetic dipoles moment can be neglected compared to the Lorentz force. Also, the viscous dissipation, radiation effects and Joule heating are supposed to be insignificant.

2.2. Nanofluid thermophysical properties

Nanofluid behavior is modeled by single phase fluid. The thermophysical properties of nanofluid are defined as follows [58]:

$$\rho_{nf} = (1-\phi)\rho_f + \phi\rho_p \tag{1}$$

$$\left(\rho C_p\right)_{nf} = (1-\phi)\left(\rho C_p\right)_f + \phi\left(\rho C_p\right)_p \tag{2}$$

$$\left(\rho\beta_T\right)_{nf} = (1-\phi)(\rho\beta)_f + \phi(\rho\beta)_p \tag{3}$$

$$\alpha_{nf} = k_{nf}\left[\left(\rho C_p\right)_{nf}\right]^{-1} \tag{4}$$

The nanofluid electrical conductivity are evaluated based on the recommendations of Sheikholeslami et al. [59]:

$$\sigma_{nf} = \sigma_f\left\{1 + \frac{3\left(\sigma_{pf}-1\right)\phi}{\left[\left(\sigma_{pf}+2\right)-\left(\sigma_{pf}-1\right)\phi\right]}\right\} \tag{5}$$

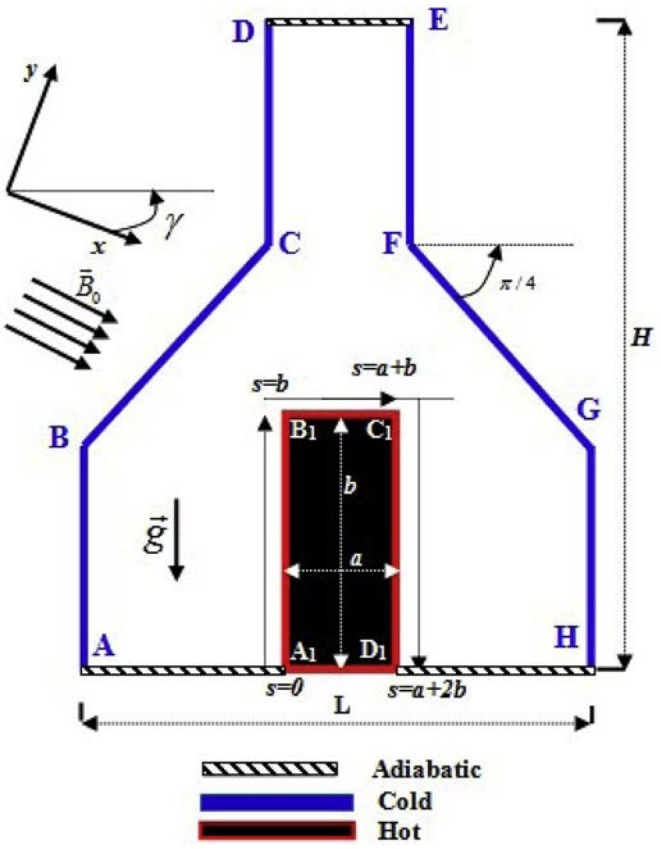

Fig. 1. Geometry of the incinerator.

Table 1
Physical properties of distilled water and Al_2O_3 [75].

	Water	Al_2O_3
ρ (kg m^{-3})	997.1	3970
Cp (J kg^{-1} K^{-1})	4179	765
K (Wm^{-1}K^{-1})	0.613	40
β (K^{-1})	2.1×10^{-4}	0.85×10^{-5}
σ (Ωm)$^{-1}$	0.05	1×10^{-10}
d_p (nm)	——-	47

Where $\sigma_{pf} = \sigma_p/\sigma_f$

With respect to thermal conductivity, Koo and Kleinstreuer [60] represented a model which was revised by Li [61] and comprised the effect of Brownian motion, nanoparticle concentration, nanoparticle size and nanofluid temperature [62] (Table 1):

$$k_{eff} = k_{static} + k_{Brownian} \tag{6}$$

$$k_{static} = k_f\frac{\left[k_p + 2k_f - 2\phi\left(k_f - k_p\right)\right]}{\left[k_p + 2k_f + \phi\left(k_f - k_p\right)\right]} \tag{7}$$

$$k_{Brownian} = 5\times10^4\phi\rho_f C_{p,f}\sqrt{\frac{k_b T}{\rho_p d_p}}g'\left(T,\phi,d_p\right) \tag{8}$$

where the function $g'(T, \varphi, d_p)$ is given by:

$$g'\left(T,\phi,d_p\right) = \left(a_1 + a_2\ln(d_p) + a_3\ln(\phi) + a_4\ln(\phi)\ln(d_p) + a_5\ln\left(d_p\right)^2\ln(T)\right) + \left(a_6 + a_7\ln(d_p) + a_8\ln(\phi) + a_9\ln(\phi)\ln(d_p) + a_{10}\ln\left(d_p\right)^2\right)$$

where the coefficients a_i ($i=0,..,10$) depend on the type of nanoparticles and are given in Table 2.

Table 2
Coefficient values of Al_2O_3/water nanofluid [63].

a_1	52.813488759
a_2	6.115637295
a_3	0.6955745084
a_4	$4.17455552786 \times 10^{-2}$
a_5	0.176919300241
a_6	−298.19819084
a_7	−34.532716906
a_8	−3.9225289283
a_9	−0.2354329626
a_{10}	−0.999063481

The nanofluid effective viscosity can be calculated from the suggested formula by Sheikholeslami and Ganji [63]. This model is valid for dilute suspensions ($\varphi \leq 4\%$) containing tiny spherical particles:

$$\mu_{eff} = \mu_{static} + \mu_{Brownian} = \mu_{static} + \frac{k_{Brownian}}{k_f} \times \frac{\mu_f}{\mathrm{Pr}_f} \tag{9}$$

$$\mu_{static} = \mu_f (1-\phi)^{-2.5} \tag{10}$$

where μ_{static} is the nanofluid viscosity calculated from Brinkman [64] equation.

3. Lattice Boltzmann Method

The Lattice Boltzmann Method (LBM) is based on Ludwig Boltzmann's kinetic theory of gases. The main idea of this model is that fluids can be considered as a lot of tiny particles moving with random motions. The main variable in LBM algorithm is the density distribution function $f_i(x, t)$ of the fluid pseudo-molecules that has lattice velocity c_i at location x and time t [35]. The lattice Boltzmann equation with Bhatnagar–Gross–Krook (BGK) approximation, for incompressible problems, utilizes two distribution functions; f and g, for the flow (f) and temperature fields (g), respectively. Concerning the flow field, the discretized LBM equations can be obtained by [63]:

For the flow field:

$$f_i\left(\mathbf{x} + \mathbf{c_i}\Delta t, t + \Delta t\right) = f_i(\mathbf{x}, t) - \frac{1}{\tau_v}\left(f_i(\mathbf{x}, t) - f_i^{\mathrm{eq}}(\mathbf{x}, t)\right) + \Delta t \mathbf{c_i} F_i \tag{11}$$

For the temperature field:

$$\mathrm{g}_i\left(\mathbf{x} + \mathbf{c_i}\Delta t, t + \Delta t\right) = \mathrm{g}_i(\mathbf{x}, t) - \frac{1}{\tau_\alpha}\left(\mathrm{g}_i(\mathbf{x}, t) - \mathrm{g}_i^{\mathrm{eq}}(\mathbf{x}, t)\right) \tag{12}$$

Where Δt refers to lattice time step which is set to 1. The left side of Eq. (11) is often called streaming or propagation and used for calculation of migration of fluid molecules from one node to its neighbor grid point. The collision part (right side) calculates the relaxation process of the molecules to the local equilibrium distribution f_i^{eq}, namely the truncated Boltzmann distribution when the BGK collision model is used.

$$f_i^{\mathrm{eq}} = \omega_i \rho \left[1 + \frac{3(\mathbf{c_i}.\mathbf{u})}{c^2} + \frac{9(\mathbf{c_i}.\mathbf{u})^2}{2c^4} - \frac{3\mathbf{u}^2}{2c^2}\right] \tag{13}$$

$$\mathrm{g}_i^{\mathrm{eq}} = \omega_i' T \left[1 + 3\frac{(\mathbf{c_i}.\mathbf{u})}{c^2} + \frac{9(\mathbf{c_i}.\mathbf{u})^2}{2c^4} - \frac{3\mathbf{u}^2}{2c^2}\right] \tag{14}$$

where u and ρ are the macroscopic velocity and density, respectively. The double populations D2Q9-D2Q9 thermal model is applied in this study. Thus, the discrete particle velocity vectors and the weighting factors are given as follows:

For D2Q9

$$\mathbf{c_i} = \begin{cases} 0 & i = 0 \\ (\cos[(i-1)\pi/2], \sin[(i-1)\pi/2])c & i = 1,2,3,4 \\ \sqrt{2}(\cos[(i-5)\pi/2 + \pi/4], \sin[(i-5)\pi/2 + \pi/4])c & i = 5,6,7,8 \end{cases} \tag{15}$$

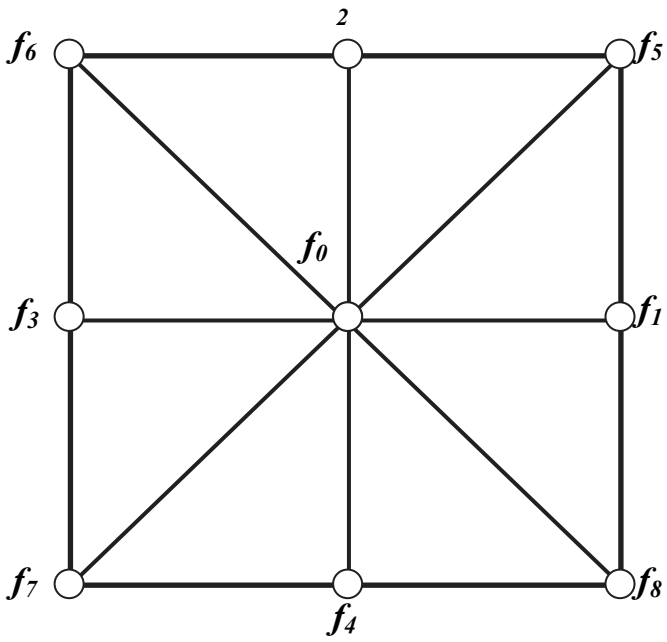

Fig. 2. Domain boundaries and direction of streaming velocities, D2Q9.

$$\omega_0 = \frac{4}{9},$$
$$\omega_i = \frac{1}{9} \text{ for i} = 1,2,3,4 \text{ and}$$
$$\omega_i = \frac{1}{36} \text{ for i} = 5,6,7,8 \tag{16}$$

The thermal diffusivity α and kinematic viscosity ν are respectively related to the relaxation time by equation below:

$$\alpha = \left[\tau_\alpha - \frac{1}{2}\right]{c_s}^2 \Delta t, \quad \nu = \left[\tau_\nu - \frac{1}{2}\right]{c_s}^2 \Delta t \tag{17}$$

where c_s is the speed of sound inside the lattice which is equal to $c_s = c/\sqrt{3}$.

In the case of free convection study, the external force term F_i is given by equation below:

$$F_i = \frac{\omega_i}{{c_s}^2} F.c_i \tag{18}$$

where F is the total external body force.

Macroscopic quantities ρ, u and T can be calculated respectively by equations below.

$$\rho = \sum_i f_i \tag{19}$$

$$\rho u = \sum_i f_i \mathbf{c_i} \tag{20}$$

$$T = \sum_i \mathrm{g}_i \tag{21}$$

3.1. Boundary conditions

By considering Fig. 1, the boundary conditions of flow field are calculated as follows:

Incinerator walls $AB, BC, CD, DE, EF, FG, GH, HA$: $U = V = 0$
Incinerator walls AB, BC, CD, EF, FG, GH: $T = T_c$
Incinerator walls DE, HD_1, A_1A: $\partial T/\partial y = 0$
Hot block walls, $A_1B_1, B_1C_1, C_1D_1, D_1A_1$: $U = V = 0, T = T_h$

Therefore, by using the bounce-back scheme at the boundary nodes (Fig. 2), the outer distribution functions from the domain are recognized by the streaming process and the inner ones are determined as follows for the flow B.C.s:

$AB, CD, C_1D_1 : f_1 = f_3, f_5 = f_7, f_8 = f_6$
$BC : f_1 = f_3, f_4 = f_2, f_8 = f_6$
$DE : f_4 = f_2, f_8 = f_6, f_7 = f_5$
$EF, GH, A_1B_1 : f_3 = f_1, f_7 = f_5, f_6 = f_8$
$FG : f_3 = f_1, f_4 = f_2, f_7 = f_5$
and $AH, B_1C_1 : f2 = f_4, f_5 = f_7, f_6 = f_8$.

The thermal boundary conditions are considered as follows:

$AB, CD : g_1 = -g_3, g_5 = -g_7, g_8 = -g_6,$
$BC : g_1 = -g_3, g_4 = -g_2, g_8 = -g_6,$
$DE : g_{4,n} = g_{4,n-1}, g_{7,n} = g_{7,n-1}, g_{8,n} = g_{8,n-1},$
$EF, GH : g_3 = -g_1, g_7 = -g_5, g_6 = -g_8,$
$FG : g_3 = -g_1, g_4 = -g_2, g_7 = -g_5,$
$A_1B_1 : g_3 = 2/9 - g_1, g_4 = 2/9 - g_2, g_7 = 2/9 - g_5,$
$B_1C_1 : g_1 = 2/9 - g_3, g_2 = 2/9 - g_4, g_5 = 2/9 - g_7,$
$C_1D_1 : g_2 = 2/9 - g_4, g_5 = 2/9 - g_7, g_6 = 2/9 - g_8$
and $AH : g_{2,n} = g_{2,n-1}, g_{5,n} = g_{5,n-1}, g_{6,n} = g_{6,n-1}$.

3.2. Nusselt number calculation

In LBM simulations, the Rayleigh, Prandtl and Mach numbers are attributed constants values. Consequently, the viscosity is calculated as shown in equation below.

$$v = n \times Ma \times c_s \times \sqrt{\frac{\Pr}{Ra}} \tag{22}$$

where n is the number of lattice nodes in y-direction. To guarantee the flow incompressibility, the Mach number was chosen as $\mathrm{Ma} < 0.1$ [65]. Therefore, the heat transfer coefficient is calculated as follows:

$$h = \frac{q_w}{T_h - T_c} \tag{23}$$

Local Nusselt number can be obtained by [66]:

$$Nu_l = \frac{hH}{k_f} \tag{24}$$

The nanofluid thermal conductivity is expressed as [67]:

$$k_{nf} = -\frac{q_w}{\partial\theta/\partial x} \tag{25}$$

The local Nusselt number along the left wall can be expressed as a function of nanofluid and pure fluid conductivities and dimensionless temperature gradient:

$$Nu_l = -\frac{k_{nf}}{k_f}\left(\frac{\partial\theta}{\partial X}\right)\Big|_{Hot\ block} \tag{26}$$

The average Nusselt number is obtained by integrating the local Nusselt number along the hot block, as follows:

$$\overline{Nu_l} = -\frac{1}{b}\int_{A_1}^{B_1}\frac{k_{nf}}{k_f}\left(\frac{\partial\theta}{\partial X}dY\right)\Big|_{X=(L-a)/2} - \frac{1}{a}\int_{B_1}^{C_1}\frac{k_{nf}}{k_f}\left(\frac{\partial\theta}{\partial Y}dX\right)\Big|_{Y=b} - \frac{1}{b}\int_{C_1}^{D_1}\frac{k_{nf}}{k_f}\left(\frac{\partial\theta}{\partial X}dY\right)\Big|_{X=(L+a)/2} \tag{27}$$

3.3. Entropy generation equations

In the case of natural convection of magnetohydrodynamic (MHD) nanofluid flow, the associated irreversibilities are consisted of three terms [42]:

The first term ($s_{gen,h}$) is the local entropy generation because of heat transfer:

$$s_{gen,h} = \frac{k_{nf}}{T_0^2}\left[\left(\frac{\partial T}{\partial x}\right)^2 + \left(\frac{\partial T}{\partial y}\right)^2\right]$$

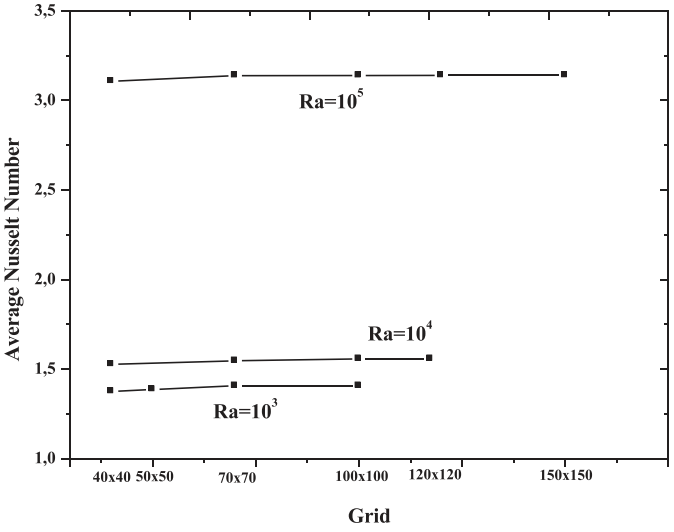

Fig. 3. Grid independency test.

Table 3
Comparison of the average Nusselt number with results of Refs. [54,68–71].

Rayleigh	10^3	10^4	10^5	10^6
Present work	1.124	2.273	4.563	8.775
Dixit and Babu [54]	1.121	2.286	4.546	8.625
Moumni et al. [68]	1.117	2.244	4.521	8.824
Kuzink et al. [69]	1.117	2.246	4.518	8.792
De Vahl Davis [70]	1.118	2.243	4.519	8.800
Djebali et al. [71]	1.115	2.226	4.508	8.713

Second term is entropy generation because of fluid friction ($s_{gen,v}$)

$$s_{gen,v} = \frac{\mu_{nf}}{T_0}\left[2\left(\frac{\partial u}{\partial x}\right)^2 + 2\left(\frac{\partial v}{\partial y}\right)^2 + \left(\frac{\partial u}{\partial y} + \frac{\partial v}{\partial x}\right)^2\right]$$

The last term ($s_{gen,\mathrm{M}}$) is local entropy generation because of the magnetic field

$$s_{gen,M} = \frac{\sigma_{nf}B_0^2}{T_0}v^2$$

The total entropy generation is the sum of three afromentioned entropy generations:

$$s_{gen} = s_{gen,h} + s_{gen,v} + s_{gen,M} \tag{28}$$

$$T_0 = (T_h + T_c)/2$$

The entropy generation is dimensionless using the following parameter:

$$S_{gen} = s_{gen}\frac{T_0^2H^2}{k_f(T_H - T_C)^2} \tag{29}$$

The dimensionless entropy generation averaged on the total studied medium is given by:

$$S = \frac{1}{V}\int_V S_{gen}dV \tag{30}$$

where V is the total volume of studied incinerator.

3.4. Grid independency study and validation

To ensure the grid independence, the sensitivity of present results is examined for five different uniform grids: 50×50, 80×80, 100×100, 120×120 and 150×150. It is found that a grid of 100×100 can be

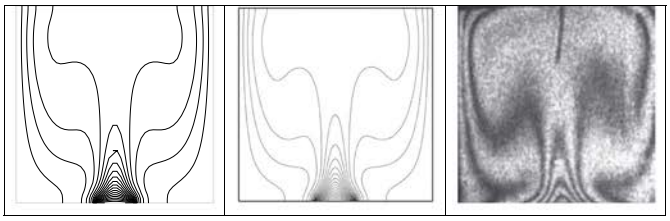

(a) Comparison of temperature distribution: (left) Present code, (middle) CIP thermal lattice-Boltzmann method[72] and (right) experimental[43] (Ra = 2.02×10^5).

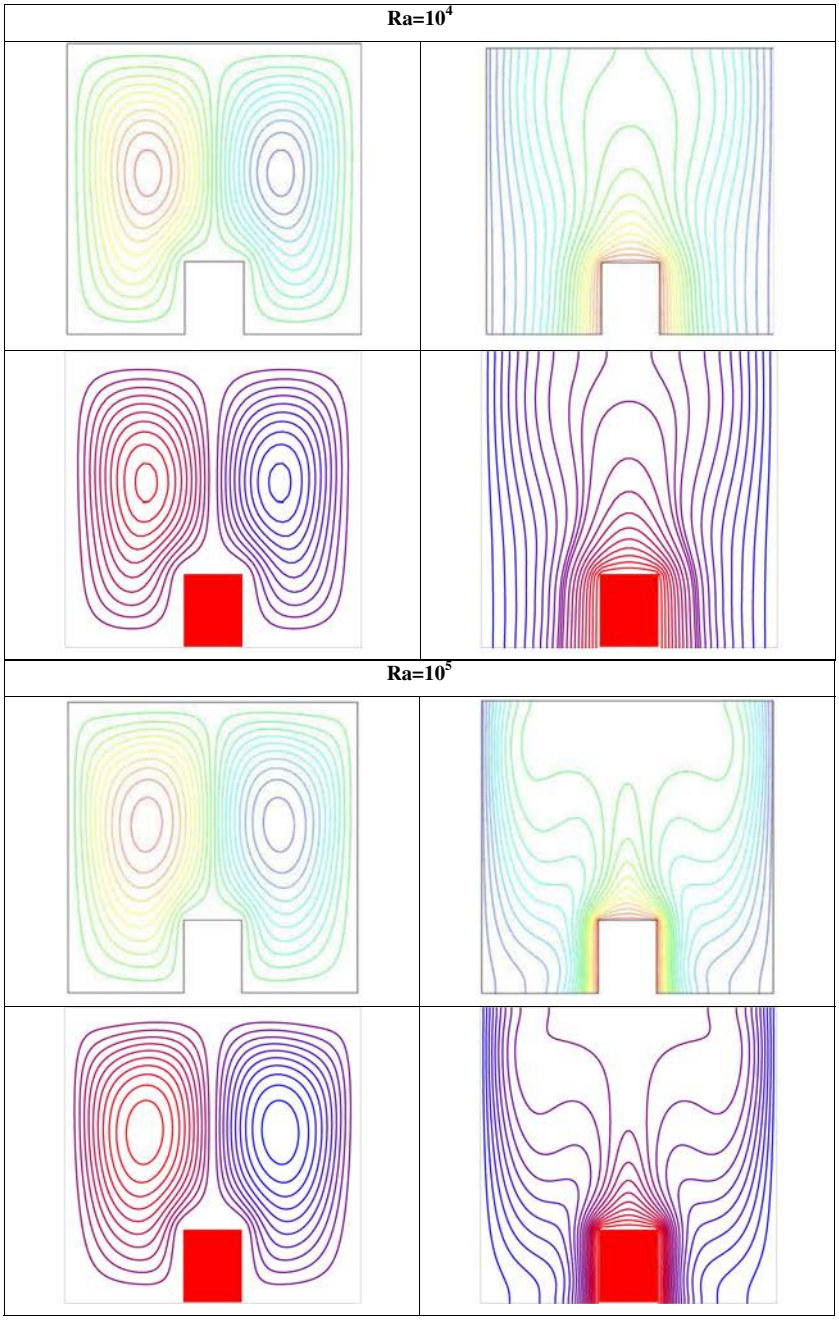

(b) Comparison of the streamlines and isotherms between the present LBM results and the numerical results of AlAmiri, Khanafer and Pop [73].

Fig. 4. Validation with previous studies.

used for Rayleigh numbers equal to $Ra = 10^3$ and $Ra = 10^4$. In case of higher Rayleigh numbers, a more refined mesh is needed to obtain a grid independent solution (Fig. 3). For $Ra = 10^5$, the chosen grid is equal to 120×120.

Table 3 Gives the comparison of average Nusselt number for free convection inside a cavity with results of references [54, 68–71]. It is clear from the table that the present simulations are in acceptable agreement with previous LBM, FVM and FDM numerical findings. Fig. 4(a) demonstrates the capability of present code to peruse the laminar natural convection of air in an enclosure, in comparison with experimental data (Paroncini and Corvaro [43]) and Cubic-Interpolated-Pseudo-Particle (CIP) numerical results (Mussa et al. [72]) with minimum error. Fig. 4(b) demonstrates the comparison of isotherms and streamlines obtained from present LBM code with results of AlAmiri et al. [73]. In that work, they have investigated the laminar free convection heat transfer in a partially divided square enclosure using finite element method. Comparisons have been done for Rayleigh numbers equal to 10^4 and 10^5. It is clear from the figure that the predictions of present model are in good agreement with AlAmiri et al. [73].

4. Results and discussion

Heat transfer inside the incinerator cavity with a hot block located on the bottom wall can be divided into three zones; the first is between the right side of the hot block and the right side of the incinerator vertical wall where it is considered as the case of differentially heated cavity opened at the top, the second zone is similar to the first one but located on the left part. The third zone is placed on the top of the heated block which can be considered as the Rayleigh–Bénard convection.

Fig. 5 presents the influence of Rayleigh number on streamlines, and isotherms inside the incinerator, filled with distilled water ($\phi = 0\%$, dashed lines) and Al_2O_3–water nanofluid ($\phi = 4\%$, solid lines), and for three values of Hartmann number (Ha = 0, 40, 100). The results demonstrated that if Hartmann number enhances, the intensity of clockwise recirculating cell inside the cavity weakens for either fluids or nanofluids. This decrease is more accentuated for higher Rayleigh numbers. The thickness of thermal boundary layer near the hot block vertical walls has a direct, ascending relation with Hartmann number, due to the magnetic field which is weakening the flow. The convection mechanism on the hot block walls vanishes as the intensity of magnetic field increases.

For $Ra = 10^3$, the isotherms are parallel to the hot block faces showing pure conduction heat transfer regime and adding more nanoparticles to base fluid do not have any considerable influence on temperature profiles. Inside the incinerator, two symmetric vortexes are created. The left cell is rotated counterclockwise and the value of stream function is 2.601×10^{-2} for distilled water. The right cell is rotated clockwise and the value of its stream-function is equal to -2.601×10^{-2} for the same working fluid. For nanofluid, the shape of streamlines (with a slightly extension at the top of vortexes) is the same as distilled water, although the lowest and highest values of stream-function are decreased to $\Psi_{max,nf} = 2.246 \times 10^{-2}$ and $\Psi_{min,nf} = -2.246 \times 10^{-2}$. This is because of the fact that the viscosity of water is lower than the viscosity of Al_2O_3/H_2O nanofluid. Therefore, the resistance of nanofluid to the flow is amplified and the friction inside the nanofluid is reinforced. The studied subject is always symmetric and the calculation of local Nusselt number shows analogous findings on the right and left walls of the block. These results are in agreement with Mliki et al. [35] findings.

Fig. 6 (a–c) depicts the local Nusselt number at the three faces of hot block as function of the Rayleigh and Hartmann numbers and for distilled water and Al_2O_3/water nanofluid. Fig. 6(a) shows that local Nusselt number is an ascending function with curvilinear abscissa on the left and right sides of hot block. This increase means that when the curvilinear abscissa leaves the adiabatic bottom, it is approached the cold sides of incinerator and therefore, the temperature gradient is augmented. Therefore, heat exchanges are augmented between hot block and the medium, whereas on the top side of hot block, the local Nusselt number has a parabolic form. The maximum heat transfer is on the top corners of the hot block (B_1, C_1, Fig. 1) whereas heat transfer is minimum on the bottom corners of heated block (A_1, D_1, Fig. 1) and on the middle of top face of hot block; because the middle of top wall of hot block is far from cold regions. Therefore, heat exchanges are minimum, compared to those between hot block vertical walls and vertical cavity cold walls. Stream function intensity is maximal on the two vortexes situated on the right and left of the hot block. In Fig. 5 and for Ha = 0, the streamlines occupy the total region on the right and left side

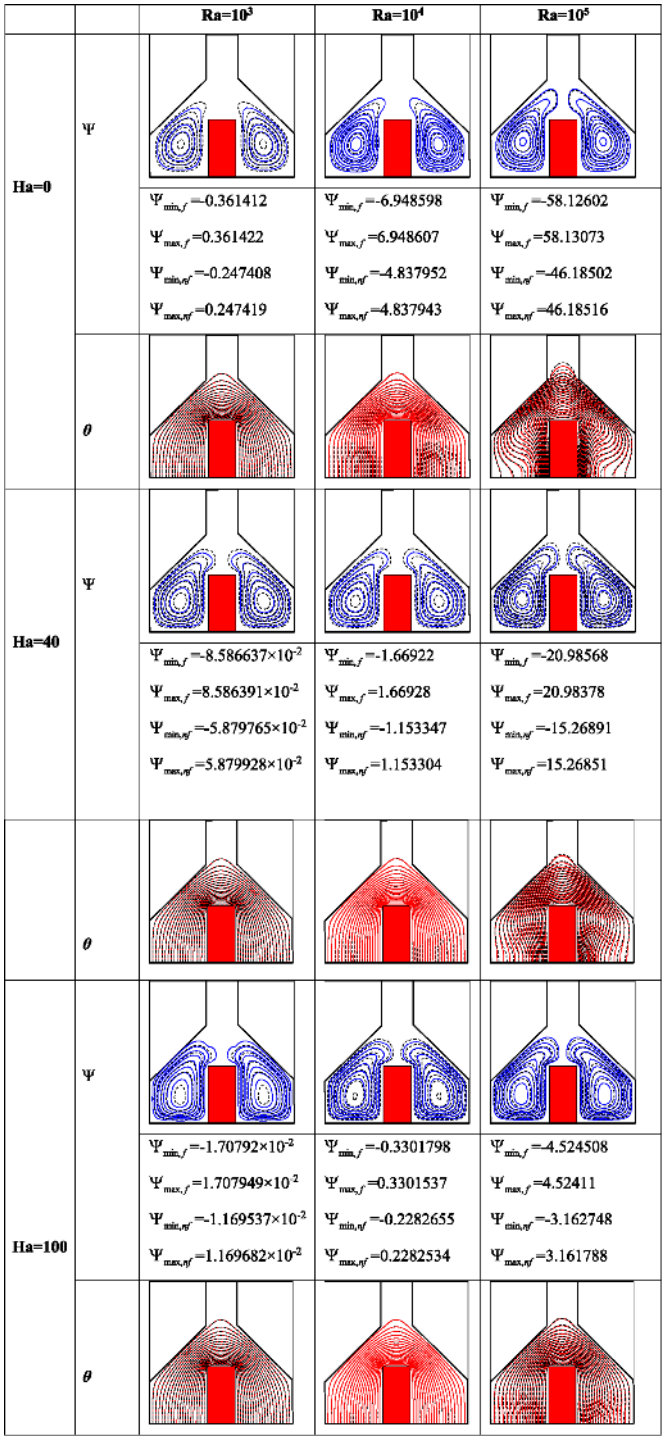

Fig. 5. Streamlines and isotherms for distilled water (dashed lines) and 4% Al_2O_3/water nanofluid (solid lines) at different Hartmann and Rayleigh numbers.

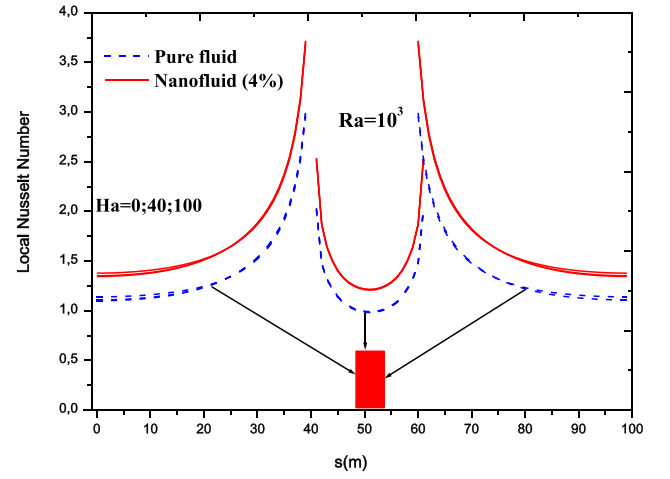

(a) Ra=10^3

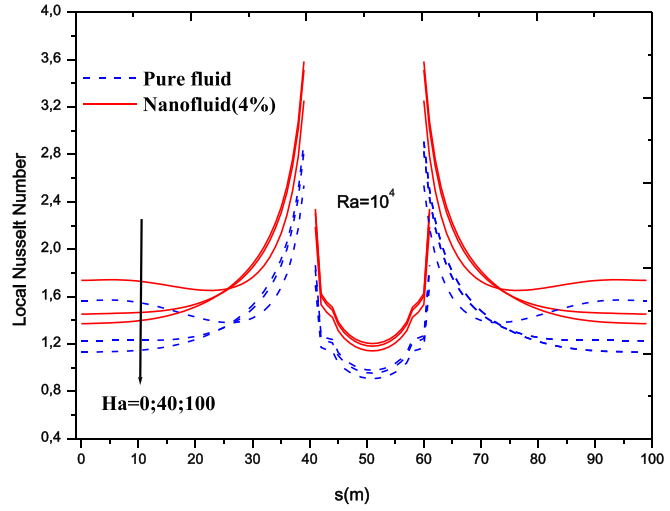

(b) Ra=10^4

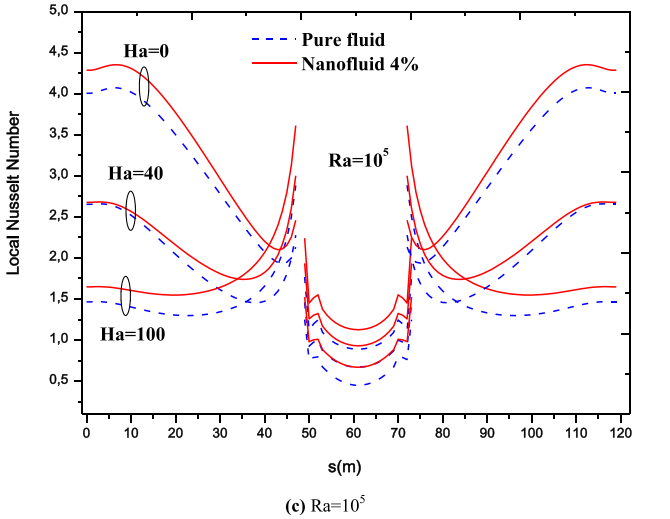

(c) Ra=10^5

Fig. 6. Effect of Hartmann number on local Nusselt number for distilled water (dashed lines) and 4% Al_2O_3–water nanofluid (solid lines).

of hot block. Therefore, heat transfer become important which its influence can be seen on local Nusselt number in Fig. 6. On the upper face of hot block, the streamlines intensity is diminished, the distance between streamlines is augmented and there is no remarkable motion on this region. Therefore, heat transfer is reduced and consequently, Nusselt number is lessened. This effect is seen for the other studied values of Hartmann number (Ha = 40 and 100) but only the shape of streamlines are different a bit. Heat transfer rate is not influenced by the magnetic field intensity and is only sensible to nanoparticle volume fraction. The variation of local Nusselt number on the hot block walls is symmetric (plane $x = 0.5$) due to the geometry, thermal and flow symmetry. Increasing the Rayleigh number to Ra = 10^4, the local Nusselt number has similar trend as the case of Ra = 10^3, but the influence of Hartmann number becomes more important showing a transition from a conductive regime to convective one. If the Hartmann number is equal to zero (Ha = 0), the local Nusselt number on the left wall presents a minimum value at the position $s = 22$ m for the nanofluid and $s = 27$ m for the distilled water. On the top of hot block, the local Nusselt number has a parabolic shape which turns its concavity to the incinerator bottom.

When the Rayleigh number is equal to Ra = 10^5 and Hartmann numbers are equal to Ha = 0 or 40, the local Nusselt number has a descending trend with respect to curvilinear abscissa. The local Nusselt number increases when the horizontal hot wall is approached. But, if the Hartmann number is equal to Ha = 100, the profile of local Nusselt number is the same as the case for Ra = 10^3. The regime is a pure convective for Ha = 0 and 40, while the magnetic field is applied (Ha = 100), the strong effect of magnetic field can be perfectly seen. In fact, the heat exchanges are reduced while the Hartmann number is enhanced to 100 and the local Nusselt number for this case shows a pure conductive regime even when the Rayleigh number is equal to $Ra = 10^5$.

Table 4 gives the average Nusselt number for distilled water and nanofluid on the left wall of hot block, as a function of Hartmann and Rayleigh numbers. It is resulted from this table that the Nusselt number is a descending function with the Hartmann number. This decrement is well pronounced for higher Rayleigh numbers where the convection heat transfer mode is predominant. For all considered Hartmann and Rayleigh numbers, the Nusselt number is an ascending function with nanoparticle volume fraction. Also, the average Nusselt numbers have higher values for nanofluids, compared to distilled water.

Fig. 7 presents the influence of the incinerator inclination angle (γ) and solid volume fraction (φ) on the isotherms and streamlines. The Rayleigh number and hot block height are chosen equal to Ra = 10^5 and 0.4, respectively, while the inclination angle varies from 0 to 180°. For $\gamma = 45°$, 60°, the dynamic structure is typified by three cells of different shapes and dimensions at the left, right and top of hot block. The left and top cells are linked and rotate counter clockwise. The right cell takes the form of surrounding space and is clockwise rotating. Compared to the $\gamma = 0°$ case, the thermal structure has widely changed at right of hot block, for inclined cases. Besides, it is worth noting that adding nanoparticles does not affect the pure dynamic and thermal structure for $\gamma = 45°$, 60° tilting cases. For a quarter turn rotation ($\gamma = 90°$), the streamlines for the distilled water are formed by two eddies, whereas for nanofluid, these two eddies are merged on one big eddy occupying the whole medium. Increasing continuously the inclination angle, two eddies are obtained again for the distilled water and nanofluid and the head of top cell begins to merge with the right cell and form a large cell extended from right to top of the heater. The dimension of the large cell diminishes as the inclination angle approaches 180° where two equal, symmetric cells are obtained.

Fig. 8 demonstrates the impact of inclination angle on average Nusselt number around the heater for both cases of base fluid and nanofluid ($\varphi = 4\%$). In the top side of heat source, three zones are distinguished: for $0 \le \gamma \le 150°$, the average Nusselt number enhances as the inclination angle augments. $150° \le \gamma \le 220°$, the average Nusselt number is nearly constant with the inclination angle. For $220° \le \gamma \le 360°$, the av-

Table 4
Average Nusselt number on the left wall of heated block.

Ha		Nu_{av}					
		0	20	40	60	80	100
10^3	Distilled water	1.416633	1.412893	1.410053	1.408839	1.408276	1.407975
	Nanofluid	1.733509	1.730459	1.728035	1.727018	1.726529	1.726285
10^4	Distilled water	1.556125	1.481316	1.436567	1.421496	1.415005	1.411618
	Nanofluid	1.836309	1.781176	1.747206	1.735139	1.729791	1.726943
10^5	Distilled water	3.144289	2.666786	2.015617	1.694949	1.565028	1.506712
	Nanofluid	3.373514	2.830573	2.203377	1.946752	1.849503	1.805766

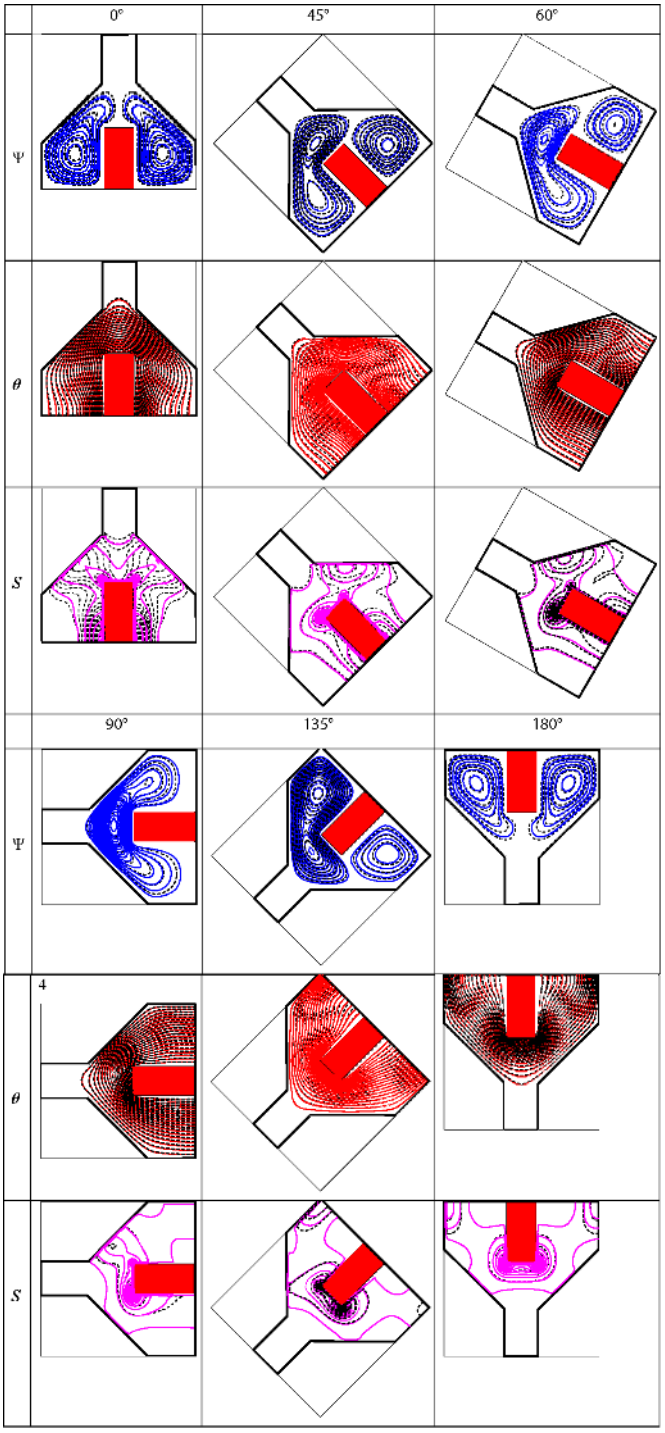

Fig. 7. Effect of incinerator inclination angle (γ) on streamlines, isotherms and local entropy generation, Ha = 40 and Ra = 10^5 (— φ = 4% nanofluid (solid lines); - - - - Base fluid (dashed lines)).

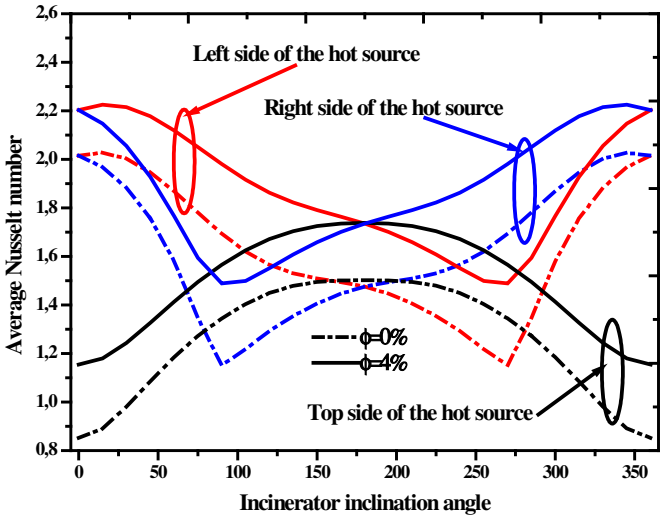

Fig. 8. Effect of incinerator inclination angle (γ) on average Nusselt number at the left, right and top sides of the hot block for Ha = 40 and Ra = 10^5 (— φ = 4% nanofluid (solid lines); - - - - Base fluid (dashed lines)).

erage Nusselt number reduces with the inclination angle increase. The Nusselt number in the case of the right and left sides diminishes with expanding inclination angle for $0^\circ \le \gamma \le 90^\circ$ and enhances when the inclination angle is increased for $270^\circ \le \gamma \le 360^\circ$. In $90^\circ \le \gamma \le 270^\circ$, the Nusselt number varies sinusoidally as the inclination angle raises for the left or right side of heat source. Besides, it is observed that the inclination angle is a key factor on heat transfer in the three sides of heat source.

Fig. 9 depicts local entropy generation (S_{gen}) for distilled water and 4% alumina/Water nanofluid, at different Ra and Ha. For Ra = 10^3, the entropy generation is maximum at the top corners of the hot block. It is discovered that for all the cases, the entropy generation raises by nanoparticles volume fraction augmentation due to the increase of irreversibility factor. This can be explicated by the augmentation of effective thermal conductivity, viscosity and electrical conductivity which appear in total entropy generation formula (Eq. (28)). For Ha = 0, if the Rayleigh number is increased from 10^3 to10^5, the maximum values of total entropy generated for distilled water are decreased from 2.014×10^{-2} to 7.195×10^{-3}, respectively. The maximum entropy generated for nanofluid is greater than its value for distilled water for all studied Rayleigh numbers. Also, it can be concluded that total entropy generation augments by Hartmann number reduction or enhancing the Rayleigh number.

Fig. 10 shows the effect of Hartmann number on normalized entropy generation (S_{gen}(Ha)/S_{gen}(Ha = 0)) for different Rayleigh numbers. For low Rayleigh numbers, it is shown that the normalized entropy generation slightly decreases with the Hartmann number. If the Rayleigh number is increased to Ra = 10^5, the rate of decrement becomes faster and the normalized total entropy generation becomes a descending function with Hartmann number.

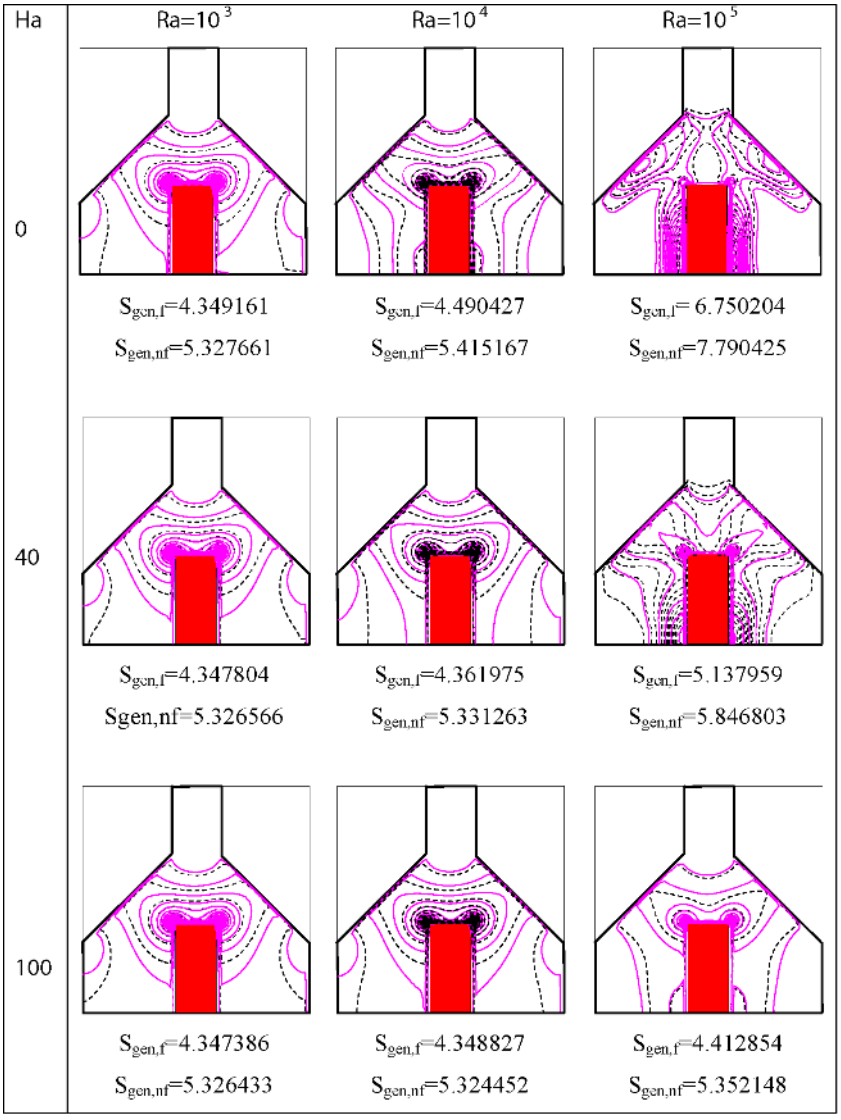

Fig. 9. Local entropy generation for distilled water (dashed lines) and 4% Al_2O_3/water nanofluid (solid lines) at different Rayleigh and Hartmann numbers.

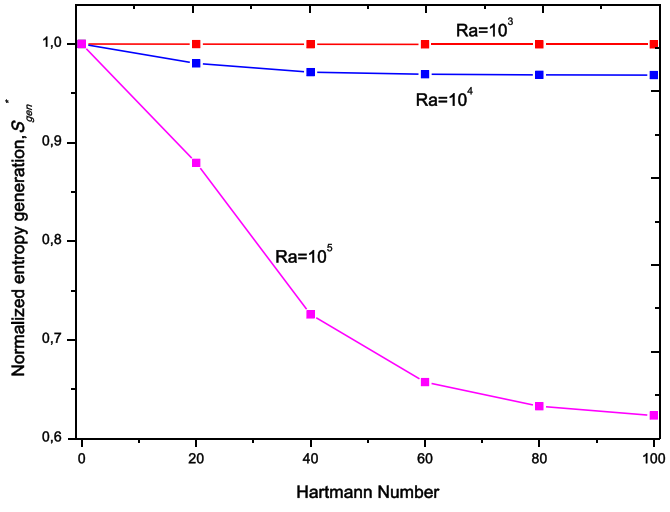

Fig. 10. Effect of Hartmann number on normalized entropy generation for different Rayleigh numbers.

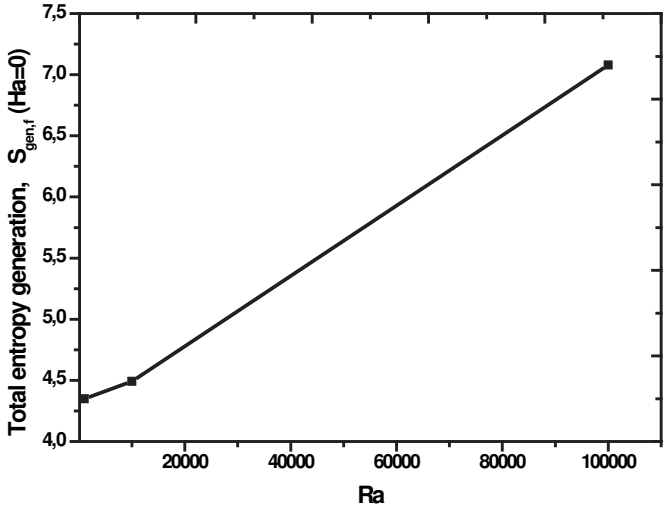

Fig. 11. Variation of total entropy generation versus Ra ($\varphi = 4\%$).

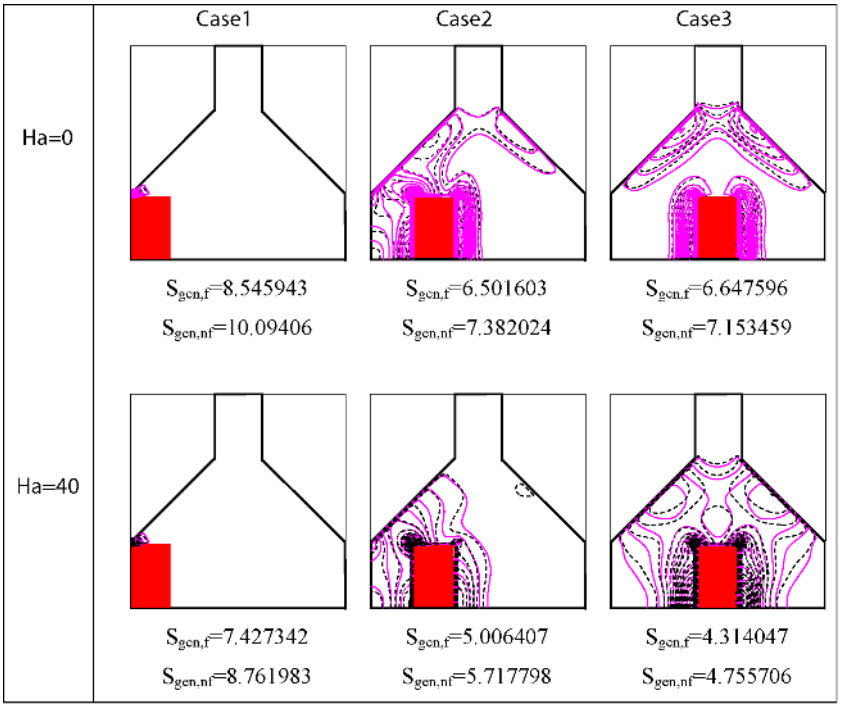

Fig. 12. Effect of hot block position on local entropy generation at $Ra = 10^5$; for distilled water (dashed lines) and 4% Al_2O_3/water nanofluid (solid lines).

Fig. 11 illustrates the variation of total entropy generation versus Rayleig hnumber for Ha = 0. As can be seen from the figure, total entropy generation is an increasing function with Ra. In fact, as the Rayleigh number augments, the conduction mechanism gradually transits to a convection mechanism, the streamlines intensity boostes and a stronger temperature gradient is constructed inside the incinerator domain. As a result, the fluid friction irreversibility and heat transfer irreversibility impacts become more visible and therefore, the total entropy generation amplified [74]. The curve slope between $Ra = 10^4$ and 10^5 is greater than the curve slope between $Ra = 10^3$ and 10^4. It means that entropy generation is enhanced more intensively in higher Rayleigh numbers.

Fig. 12 depicts the impact of hot block position on local entropy generation at Rayleigh number $= 10^5$. The figure depicted that the maximum entropy generated is for case 1 (heater attached to the left wall of incinerator) and the minimum entropy generated is found for case 3 (heater located at the middle of lower wall). All this can be explicated by the fact that for case 1, the hot block is located near the cold and non-slip wall. Therefore, temperature and velocity gradients are considerable, whereas for case 3, the hot block is situated far from the cold wall. Therefore, velocity and temperature gradients are minimized. For all considered cases, entropy generation augments with Hartmann number decrement and nanoparticle volume fraction increment.

Fig. 13 depicts the effect of incinerator inclination angle (γ) on local entropy generation for $Ra = 10^5$ and Ha = 40. Diagrams are symmetric with respect to $\gamma = 180^\circ$ and it can be divided into three zones. The first is situated between 0° to 90°, where the total entropy generation has a descending trend with respect to incinerator inclination angle. Then, in the range between 90° and 270°, it has a parabolic shape which turns its concavity to the top of incinerator with a maximum at$\gamma = 180^\circ$. The third zone is located between 270° and 360° where the total entropy generation is a boosting function with the inclination angle. This curve represents three maximums which are on $\gamma = 15^\circ$, 180°, and 345° and two minimums at $\gamma = 90^\circ$ and 270°. The total entropy generation for nanofluid is superior to the case of distilled water. This curve associated with Fig. 8 shows that for the top wall of hot block, the best compromise between maximum heat transfer and entropy generation minimization is to take $\gamma = 90^\circ$ or 270°; whereas, for the left and right walls of hot block, a maximum heat transfer is accompanied by a maximum entropy generation.

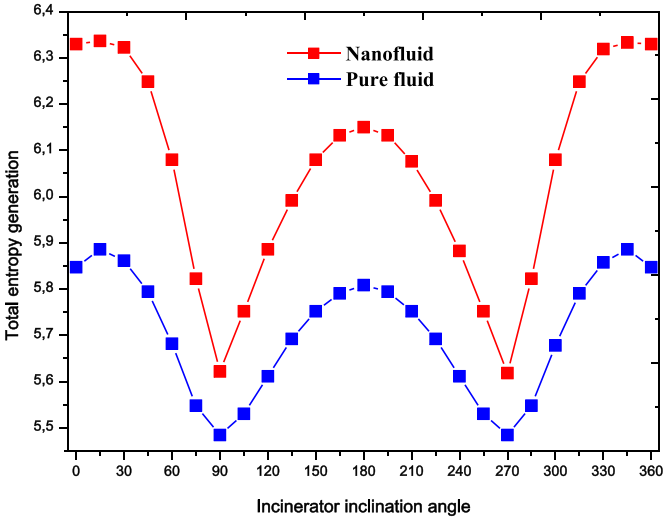

Fig. 13. Effect of incinerator inclination angle (γ) on total local entropy generation of distilled water and 4% alumina/water nanofluid at Ha = 40 and $Ra = 10^5$.

Fig. 14(a) shows the influence of relative heat source height on local entropy generation for Ha = 40, $Ra = 10^3$–10^5 and for distilled water and nanofluid. The relative heat source is varied from 0.1 to 0.5. It can be seen that the entropy generation is an ascending function with the relative heat source height as well as Rayleigh number. This increment is well pronounced for high Rayleigh numbers. This can be explained by the fact that if the hot block relative height is increased, the hot walls approach the cold one. Due to more energy which will be transferred to the cold walls, temperature and velocity gradients increase. This is also well explained by Fig. 14(b).

Fig. 15(a) illustrates the influence of relative hot source width on local entropy generation for $Ra = 10^3$–10^5 and Ha = 40. The relative hot

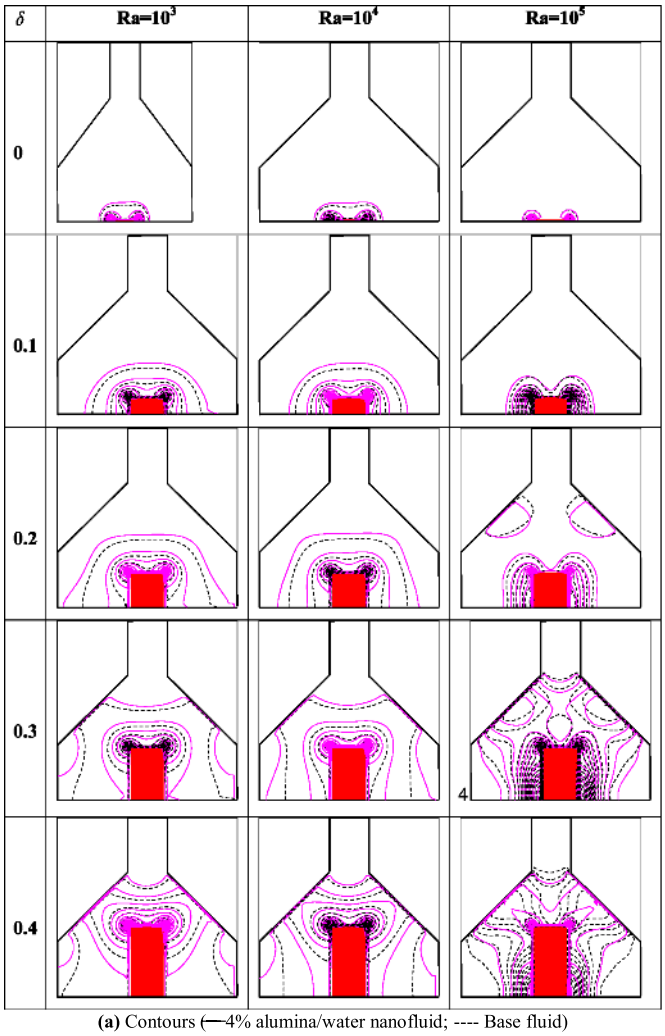

(a) Contours (—4% alumina/water nanofluid; ---- Base fluid)

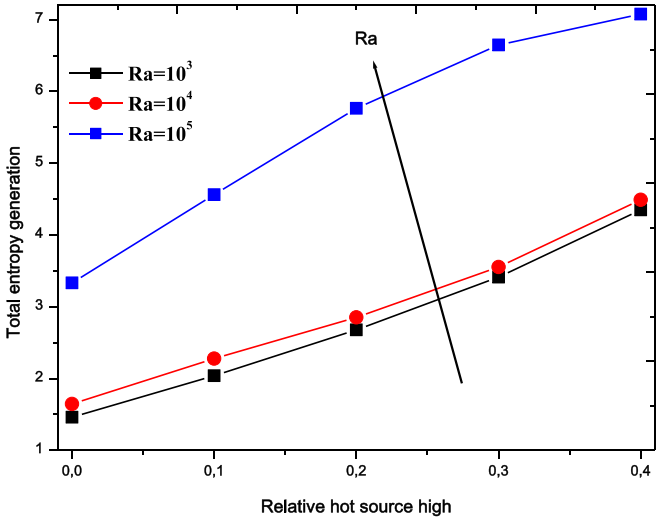

(b)

Fig. 14. Effect of relative hot block height on total entropy generation (Ha = 40).

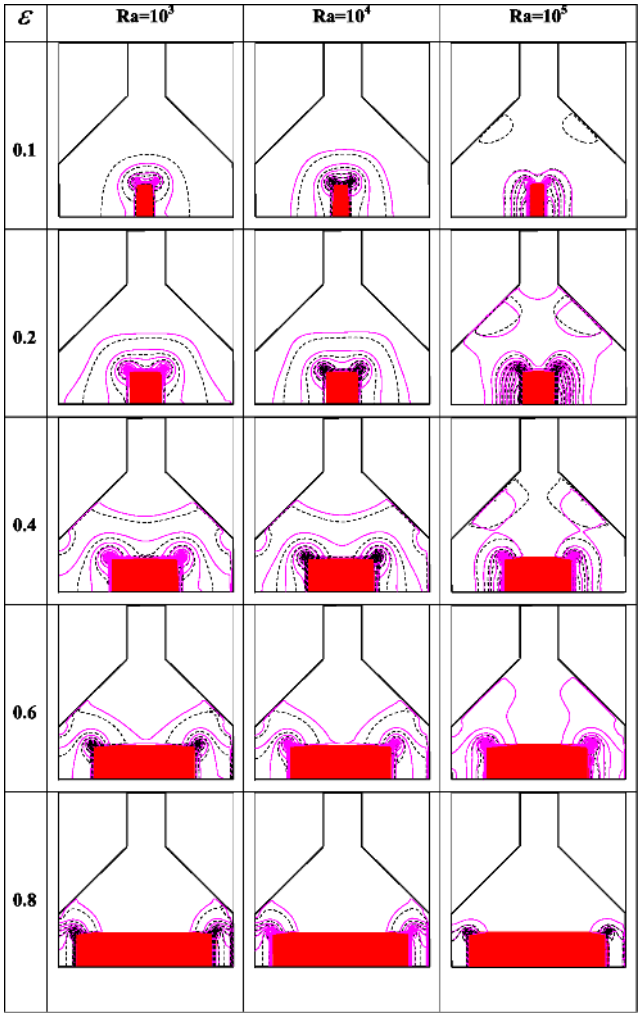

(a) Contours (— 4% alumina/water nanofluid; ---- Base fluid)

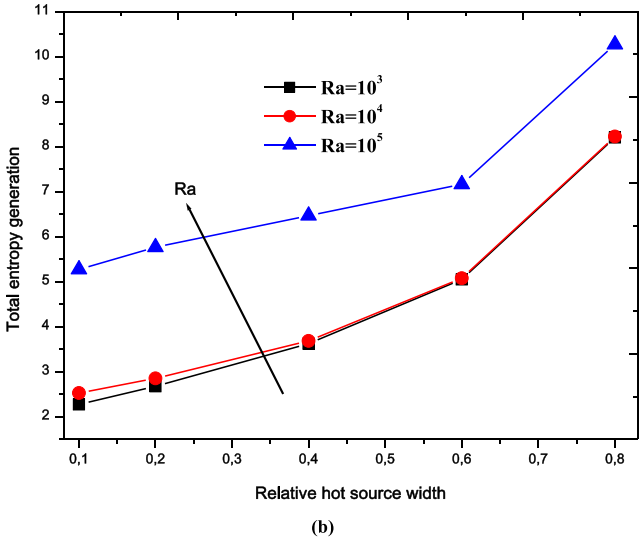

(b)

Fig. 15. Effect of relative hot block width on total entropy generation (Ha = 40).

source width is varied from 0.1 to 0.8. Here, the total entropy generation is a growing function with Rayleigh number and relative hot block width. This result is confirmed by Fig. 15(b). For all studied Rayleigh numbers, trends of diagrams are same. The entropy generation increases gradually for the relative hot source width varying from 0.1 to 0.6, then,

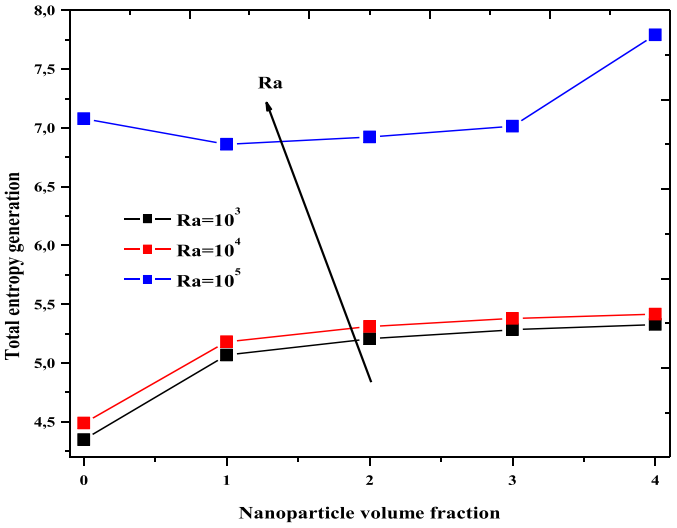

Fig. 16. Effect of nanoparticle volume fraction on total entropy generation (Ha = 0).

the increasing trend becomes faster due to the temperature and velocity steep gradients, when approaching cold faces.

Fig. 16 shows the total entropy generation for different Rayleigh numbers, volume fraction of nanoparticles and Ha = 0. Total entropy generation enhances as the volume fraction of nanoparticles augments. This increase is due to the augmentation of the effective viscosity and thermal conductivity of the nanofluid which leads to heat transfer and fluid friction enhancement. This increment becomes more considerable by Rayleigh number augmentation.

5. Conclusion

A numerical study using the Lattice Boltzmann Method has been accomplished to determine the fluid flow, thermal and entropy generation characteristics associated with the MHD natural convection in an incinerator shaped enclosure containing a hot rectangular block. Results were presented and discussed for flow structure, isotherms, local and average Nusselt number, and local as well as total entropy generation. Parametric study was carried out for different parameters such as Rayleigh number, nanoparticles volume fraction, hot block dimensions (height and width), hot block position, Hartmann number, and incinerator inclination angle. The most substantial results of the present study are as follows:

- If the Hartmann number augments, the intensity of clockwise recirculating cell inside the cavity weakens for either fluids or nanofluids. This decrease is more accentuated for higher Rayleigh numbers.
- The thickness of thermal boundary layer near the vertical walls of hot block has a direct, ascending relation with the Hartmann number, due to the magnetic field which is weakening the flow.
- Heat transfer rate is not influenced by the magnetic field intensity and is only sensible to nanoparticle volume fraction.
- Applying magnetic field, convection heat transfer is reduced. This phenomenon is more pronounced for higher Rayleigh numbers.
- Nusselt number is a descending function with the Hartmann number.
- Maximum heat transfer is on the top corners of hot block. Whereas heat transfer is minimum on the bottom corners of heated block.
- The incinerator inclination angle is found to be a key parameter to control the heat transfer for both distilled water and nanofluid. The best compromise between maximum heat transfer and entropy generation minimization is to take $\gamma = 90^\circ$ or 270°.
- Increasing the hot block height or width causes an enhancement of the heat transfer for all tested cases.
- The total entropy generated is an ascending function with relative hot block height, relative hot block width, nanoparticle volume fraction and Rayleigh number. This increase is well pronounced for higher Rayleigh numbers. However, entropy generation decreases with increasing Hartmann number.

Conflict of interests

The authors declare that there is no conflict of interests regarding the publication of this paper.

References

[1] Siddique M, Khaled A-R, Abdulhafiz N, Boukhary A. Recent advances in heat transfer enhancements: a review report. Int J Chem Eng 2010;2010:1–28.
[2] Bergles A. The implications and challenges of enhanced heat transfer for the chemical process industries. Chem Eng Res Des 2001;79:437–44.
[3] Choi SUS, Eastman Ja. Enhancing thermal conductivity of fluids with nanoparticles. In: Proceedings of ASME International Mechanical Engineering Congress & Exposition. San Francisco, CA, USA: ASME-Publications-Fed; 1995. p. 99–106.
[4] Safaei MR, Safdari Shadloo M, Goodarzi MS, Hadjadj A, Goshayeshi HR, Afrand M, Kazi S. A survey on experimental and numerical studies of convection heat transfer of nanofluids inside closed conduits. Adv Mech Eng 2016;8:1–14.
[5] Shamshirband S, Malvandi A, Karimipour A, Goodarzi M, Afrand M, Petković D, Dahari M, Mahmoodian N. Performance investigation of micro-and nano-sized particle erosion in a 90° elbow using an ANFIS model. Powder Technol 2015;284:336–43.
[6] Heydari A, Akbari OA, Safaei MR, Derakhshani M, Alrashed AAAA, Mashayekhi R, Ahmadi Sheikh Shabani G, Zarringhalam M, Nguyen TK. The effect of attack angle of triangular ribs on heat transfer of nanofluids in a microchannel. J Therm Anal Calorim 2018;131:2893–912.
[7] Sheikholeslami M, Gorji-Bandpy M. Free convection of ferrofluid in a cavity heated from below in the presence of an external magnetic field. Powder Technol 2014;256:490–8.
[8] Sarafraz MM, Arya A, Hormozi F, Nikkhah V. On the convective thermal performance of a CPU cooler working with liquid gallium and CuO/water nanofluid: a comparative study. Appl Therm Eng 2017;112:1373–81.
[9] Hemmat Esfe M, Saedodin S, Naderi A, Alirezaie A, Karimipour A, Wongwises S, Goodarzi M, Dahari Mb. Modeling of thermal conductivity of ZnO-EG using experimental data and ANN methods. Int Commun Heat Mass Transf 2015;63:35–40.
[10] Hosseini SM, Safaei MR, Goodarzi M, Alrashed AAAA, Nguyen TK. New temperature, interfacial shell dependent dimensionless model for thermal conductivity of nanofluids. Int J Heat Mass Transf 2017;114:207–10.
[11] Salari E, Peyghambarzadeh SM, Sarafraz MM, Hormozi F. Boiling thermal performance of TiO_2 aqueous nanofluids as a coolant on a disc copper block. Period Polytech Chem Eng 2016;60:106.
[12] Goshayeshi H, Goodarzi M, Dahari M. Effect of magnetic field on the heat transfer rate of kerosene/Fe_2O_3 nanofluid in a copper oscillating heat pipe. Exp Therm Fluid Sci 2015;68:663–8.
[13] Kherbeet AS, Mohammed HA, Ahmed HE, Salman BH, Alawi OA, Safaei MR, Khazaal MT. Mixed convection nanofluid flow over microscale forward-facing step: effect of inclination and step heights. Int Commun Heat Mass Transf 2016;78:145–54.
[14] Goodarzi M, Kherbeet AS, Afrand M, Sadeghinezhad E, Mehrali M, Zahedi P, Wongwises S, Dahari M. Investigation of heat transfer performance and friction factor of a counter-flow double-pipe heat exchanger using nitrogen-doped, graphene-based nanofluids. Int Commun Heat Mass Transf 2016;76:16–23.
[15] Arani AAA, Akbari OA, Safaei MR, Marzban A, Alrashed AAAA, Ahmadi GR, Nguyen TK. Heat transfer improvement of water/single-wall carbon nanotubes (SWCNT) nanofluid in a novel design of a truncated double-layered microchannel heat sink. Int J Heat Mass Transf 2017;113:780–95.
[16] Esfe MH, Hajmohammad H, Moradi R, Arani AAA. Multi-objective optimization of cost and thermal performance of double walled carbon nanotubes/water nanofluids by NSGA-II using response surface method. Appl Therm Eng 2017;112:1648–57.
[17] Safaei M, Togun H, Vafai K, Kazi S, Badarudin A. Investigation of heat transfer enhancement in a forward-facing contracting channel using FMWCNT nanofluids. Numer Heat Transf. Part A: Appl 2014;66:1321–40.
[18] Fontes DH, Ribatski G, Bandarra Filho EP. Experimental evaluation of thermal conductivity, viscosity and breakdown voltage AC of nanofluids of carbon nanotubes and diamond in transformer oil. Diam Relat Mater 2015;58:115–21.
[19] Khodabandeh E, Safaei MR, Akbari S, Akbari OA, Alrashed AAAA. Application of nanofluid to improve the thermal performance of horizontal spiral coil utilized in solar ponds: geometric study. Renew Energy 2018;122:1–16.
[20] Prabhakaran M, Manikandan S, Suganthi K, Vinodhan VL, Rajan K. Development and assessment of ceria–propylene glycol nanofluid as an alternative to propylene glycol for cooling applications. Appl Therm Eng 2016;102:329–35.
[21] Sarafraz M, Hormozi F. Convective boiling and particulate fouling of stabilized CuO-ethylene glycol nanofluids inside the annular heat exchanger. Int Commun Heat Mass Transf 2014;53:116–23.
[22] Esfahani JA, Safaei MR, Goharimanesh M, de Oliveira LR, Goodarzi M, Shamshirband S, Filho EPB. Comparison of experimental data, modelling and non-linear regression on transport properties of mineral oil based nanofluids. Powder Technol 2017;317:458–70.
[23] Xu H, Gong L, Huang S, Xu M. Flow and heat transfer characteristics of nanofluid flowing through metal foams. Int J Heat Mass Transf 2015;83:399–407.

[24] Solangi KH, Kazi SN, Luhur MR, Badarudin A, Amiri A, Sadri R, Zubir MNM, Gharehkhani S, Teng KH. A comprehensive review of thermo-physical properties and convective heat transfer to nanofluids. Energy 2015;89:1065–86.
[25] Tanda G. Experiments on natural convection in water-cooled ribbed channels with different aspect ratios. Int J Heat Mass Transf 2017;110:606–12.
[26] Li B, Baik Y-J, Byon C. Enhanced natural convection heat transfer of a chimney-based radial heat sink. Energy Convers Manag 2016;108:422–8.
[27] Chen H-T, Chiu Y-J, Tseng H-C, Chang J-R. Effect of domain boundary set on natural convection heat transfer characteristics for vertical annular finned tube heat exchanger. Int J Heat Mass Transf 2017;109:668–82.
[28] Bahrehmand D, Ameri M. Energy and exergy analysis of different solar air collector systems with natural convection. Renewe Energy 2015;74:357–68.
[29] Yang J, Greenwood MS, Angelis MD, Avery M, Anderson M, Corradini M, Matos J, Dunn F, Feldman E. Study of critical heat flux in natural convection–cooled TRIGA reactors with single annulus and rod bundle geometries. Nucl Sci Eng 2015;180:141–53.
[30] Seifi AR, Akbari OA, Alrashed AAAA, Afshary F, Shabani GAS, Seifi R, Goodarzi M, Pourfattah F. Effects of external wind breakers of Heller dry cooling system in power plants. Appl Therm Eng 2018;129:1124–34.
[31] Fan Y, Li Y, Hang J, Wang K, Yang X. Natural convection flows along a 16-storey high-rise building. Build Environ 2016;107:215–25.
[32] Killworth PD. Deep convection in the world ocean. Rev Geophys 1983;21:1–26.
[33] Sarris I, Lekakis I, Vlachos N. Natural convection in rectangular tanks heated locally from below. Int J Heat Mass Transf 2004;47:3549–63.
[34] Esfe MH, Akbari M, Karimipour A, Afrand M, Mahian O, Wongwises S. Mixed-convection flow and heat transfer in an inclined cavity equipped to a hot obstacle using nanofluids considering temperature-dependent properties. Int J Heat Mass Transf 2015;85:656–66.
[35] Mliki B, Abbassi MA, Omri A, Zeghmati B. Effects of nanoparticles Brownian motion in a linearly/sinusoidally heated cavity with MHD natural convection in the presence of uniform heat generation/absorption. Powder Technol 2016;295:69–83.
[36] Baïri A, Zarco-Pernia E, De María J-MG. A review on natural convection in enclosures for engineering applications. The particular case of the parallelogrammic diode cavity. Appl Therm Eng 2014;63:304–22.
[37] Saravanan S, Sivaraj C. Natural convection in an enclosure with a localized nonuniform heat source on the bottom wall. Int J Heat Mass Transf 2011;54:2820–8.
[38] Öztop HF, Estellé P, Yan W-M, Al-Salem K, Orfi J, Mahian O. A brief review of natural convection in enclosures under localized heating with and without nanofluids. Int Commun Heat Mass Transf 2015;60:37–44.
[39] Abhinav R, Sunder PS, Gowrishankar A, Vignesh S, Vivek M, Kishore VR. Numerical study on effect of vent locations on natural convection in an enclosure with an internal heat source. Int Commun Heat Mass Transf 2013;49:69–77.
[40] Sheikholeslami M, Ellahi R. Three dimensional mesoscopic simulation of magnetic field effect on natural convection of nanofluid. Int J Heat Mass Transf 2015;89:799–808.
[41] Bondareva NS, Sheremet MA. Natural convection heat transfer combined with melting process in a cubical cavity under the effects of uniform inclined magnetic field and local heat source. Int J Heat Mass Transf 2017;108:1057–67.
[42] Durgam S, Venkateshan SP, Sundararajan T. Experimental and numerical investigations on optimal distribution of heat source array under natural and forced convection in a horizontal channel. Int J Therm Sci 2017;115:125–38.
[43] Paroncini M, Corvaro F. Natural convection in a square enclosure with a hot source. Int J Therm Sci 2009;48:1683–95.
[44] Mejri I, Mahmoudi A, Abbassi MA, Omri A. Magnetic field effect on entropy generation in a nanofluid-filled enclosure with sinusoidal heating on both side walls. Powder Technol 2014;266:340–53.
[45] Mejri I, Mahmoudi A, Abbassi MA, Omri A. LBM simulation of natural convection in an inclined triangular cavity filled with water. Alex Eng J 2016;55:1385–94.
[46] Mahmoudi A, Mejri I, Abbassi MA, Omri A. Analysis of the entropy generation in a nanofluid-filled cavity in the presence of magnetic field and uniform heat generation/absorption. J Mol Liq 2014;198:63–77.
[47] Kefayati GR. FDLBM simulation of entropy generation due to natural convection in an enclosure filled with non-Newtonian nanofluid. Powder Technol 2015;273:176–90.
[48] Kefayati GR. Simulation of heat transfer and entropy generation of MHD natural convection of non-Newtonian nanofluid in an enclosure. Int J Heat Mass Transf 2016;92:1066–89.
[49] Selimefendigil F, Öztop HF. Natural convection and entropy generation of nanofluid filled cavity having different shaped obstacles under the influence of magnetic field and internal heat generation. J Taiwan Inst Chem Eng 2015;56:42–56.
[50] Safaei MR, Jahanbin A, Kianifar A, Gharehkhani S, Kherbeet AS, Goodarzi M, Dahari M. Mathematical modeling for nanofluids simulation: a review of the latest works. Modeling and simulation in engineering sciences. InTech; 2016.
[51] Xu H, Xing Z. The lattice Boltzmann modeling on the nanofluid natural convective transport in a cavity filled with a porous foam. Int Commun Heat Mass Transf 2017;89:73–82.
[52] Goodarzi M, Safaei M, Karimipour A, Hooman K, Dahari M, Kazi S, Sadeghinezhad E. Comparison of the finite volume and lattice Boltzmann methods for solving natural convection heat transfer problems inside cavities and enclosures. Abstr Appl Anal 2014;2014:15.
[53] Sadeghi R, Shadloo M. Three-dimensional numerical investigation of film boiling by the lattice Boltzmann method. Numer Heat Transf. Part A: Appl 2017;71:560–74.
[54] Dixit H, Babu V. Simulation of high Rayleigh number natural convection in a square cavity using the lattice Boltzmann method. Int J Heat Mass Transf 2006;49:727–39.
[55] Succi S. The lattice Boltzmann equation: for fluid dynamics and beyond. Oxford university press; 2001.
[56] Mohamad AA. Lattice Boltzmann method: fundamentals and engineering applications with computer codes. Springer Science & Business Media; 2011.
[57] Safaei MR, Gooarzi M, Akbari OA, Shadloo MS, Dahari M. Performance evaluation of nanofluids in an inclined ribbed microchannel for electronic cooling applications. In: Murshed PSMS, editor. Electronics cooling. Croatia: InTech; 2016. p. 105–28.
[58] Goodarzi M, Safaei MR, Vafai K, Ahmadi G, Dahari M, Kazi SN, Jomhari N. Investigation of nanofluid mixed convection in a shallow cavity using a two-phase mixture model. Int J Therm Sci 2014;75:204–20.
[59] Sheikholeslami M, Bandpy MG, Ellahi R, Zeeshan A. Simulation of MHD CuO–water nanofluid flow and convective heat transfer considering Lorentz forces. J Magn Magn Mater 2014;369:69–80.
[60] Koo J, Kleinstreuer C. A new thermal conductivity model for nanofluids. J Nanopart Res 2004;6:577–88.
[61] J. Li, Computational analysis of nanofluid flow in microchannels with applications to micro-heat sinks and bio-MEMS, (2008).
[62] Wang L, Chai Z, Shi B. Regularized lattice Boltzmann simulation of double-diffusive convection of power-law nanofluids in rectangular enclosures. Int J Heat Mass Transf 2016;102:381–95.
[63] Sheikholeslami M, Ganji DD. External magnetic field effects on hydrothermal treatment of nanofluid: numerical and analytical studies. William Andrew; 2016.
[64] Brinkman H. The viscosity of concentrated suspensions and solutions. J Chem Phys 1952;20:571.
[65] Karimipour A, Hossein Nezhad A, D'Orazio A, Hemmat Esfe M, Safaei MR, Shirani E. Simulation of copper–water nanofluid in a microchannel in slip flow regime using the lattice Boltzmann method. Eur J Mech B Fluids 2015;49:89–99.
[66] Mliki B, Abbassi MA, Omri A. Lattice Boltzmann simulation of magnethydrodynamics natural convection in an L-shaped enclosure. Int J Heat Technol 2016;34:565–73.
[67] Abbassi MA, Mliki B, Djebali R. Lattice Boltzmann method for simulation of nanoparticle brownian motion and magnetic field effects on free convection in a nanofluid–filled open cavity with heat generation/absorption and non-uniform heating on the left solid vertical wall. Fluid Dyn Mater Process 2017;13:59–83.
[68] Moumni H, Welhezi H, Djebali R, Sediki E. Accurate finite volume investigation of nanofluid mixed convection in two-sided lid driven cavity including discrete heat sources. Appl Math Model 2015;39:4164–79.
[69] Kuznik F, Vareilles J, Rusaouen G, Krauss G. A double-population lattice Boltzmann method with non-uniform mesh for the simulation of natural convection in a square cavity. Int J Heat Fluid Flow 2007;28:862–70.
[70] de Vahl Davis G. Natural convection of air in a square cavity: a bench mark numerical solution. Int J Numer Methods Fluids 1983;3:249–64.
[71] Djebali R, El Ganaoui M, Sammouda H, Bennacer R. Some benchmarks of a side wall heated cavity using lattice Boltzmann approach. Fluid Dyn Mater Process 2009;164(1):261–82 1, 21 (2009).
[72] Mussa M, Abdullah S, Azwadi CN, Muhamad N. Simulation of natural convection heat transfer in an enclosure by the lattice-Boltzmann method. Comput Fluids 2011;44:162–8.
[73] AlAmiri A, Khanafer K, Pop I. Buoyancy-induced flow and heat transfer in a partially divided square enclosure. Int J Heat Mass Transf 2009;52:3818–28.
[74] Cho C-C, Chiu C-H, Lai C-Y. Natural convection and entropy generation of Al_2O_3–water nanofluid in an inclined wavy-wall cavity. Int J Heat Mass Transf 2016;97:511–20.
[75] Ghasemi B, Aminossadati S, Raisi A. Magnetic field effect on natural convection in a nanofluid-filled square enclosure. Int J Therm Sci 2011;50:1748–56.